Free electron laser stochastic spectroscopy revealing silicon bond softening dynamics

Dario De Angelis,[1,2,*] Emiliano Principi,[1] Filippo Bencivenga,[1] Daniele Fausti,[1,3,4] Laura Foglia,[1] Yishay Klein,[5] Michele Manfredda,[1] Riccardo Mincigrucci,[1] Angela Montanaro,[1,3,4] Emanuele Pedersoli,[1] Jacopo Stefano Pelli Cresi,[1] Giovanni Perosa,[1] Kevin C. Prince,[1] Elia Razzoli,[6] Sharon Shwartz,[5] Alberto Simoncig,[1] Simone Spampinati,[1] Cristian Svetina,[7] Jakub Szlachetko,[8] Alok Tripathi,[5] Ivan A. Vartanyants,[9] Marco Zangrando,[1,2] and Flavio Capotondi[1]

[1]*Elettra-Sincrotrone Trieste, Strada Statale 14-km 163.5, Basovizza, 34149, Trieste, Italy*

[2]*Istituto Officina dei Materiali, CNR, Strada Statale 14-km 163.5, Basovizza, 34149, Trieste, Italy*

[3]*Department of Physics, Università degli Studi di Trieste, 34127, Trieste, Italy*

[4]*Lehrstuhl für Festkörperphysik, Friedrich-Alexander-Universität Erlangen-Nürnberg, Erlangen 91058, Germany*

[5]*Physics Department and Institute of Nanotechnology and advanced Materials, Bar Ilan University, Ramat Gan, 52900, Israel*

[6]*Paul Scherrer Institut, CH-5232 Villigen, Switzerland*

[7]*Madrid Institute for Advanced Studies, IMDEA Nanociencia, Calle Faraday 9, Ciudad Universitaria de Cantoblanco, Madrid, 28049, Spain.*

[8]*SOLARIS National Synchrotron Radiation Centre, Jagiellonian University, Czerwone Maki 98, 30–392 Krakow, Poland*

[9]*Deutsches Elektronen-Synchrotron DESY, Notkestr. 85, 22607 Hamburg, Germany*

(Received 16 December 2022; revised 26 March 2023; accepted 22 May 2023; published 13 June 2023)

Time-resolved x-ray emission/absorption spectroscopy (Tr-XES/XAS) is an informative experimental tool sensitive to electronic dynamics in materials, widely exploited in diverse research fields. Typically, Tr-XES/XAS requires x-ray pulses with both a narrow bandwidth and subpicosecond pulse duration, a combination that in principle finds its optimum with Fourier transform-limited pulses. In this work, we explore an alternative experimental approach, capable of simultaneously retrieving information about unoccupied (XAS) and occupied (XES) states from the stochastic fluctuations of broadband extreme ultraviolet pulses of a free electron laser. We used this method, in combination with singular-value decomposition and Tikhonov regularization procedures, to determine the XAS/XES response from a crystalline silicon sample at the $L_{2,3}$ edge, with an energy resolution of a few tens of meV. Finally, we combined this spectroscopic method with a pump-probe approach to measure structural and electronic dynamics of a silicon membrane. Tr-XAS/XES data obtained after photoexcitation with an optical laser pulse at 390 nm allowed us to observe perturbations of the band structure, which are compatible with the formation of the predicted precursor state of a nonthermal solid-liquid phase transition associated with a bond softening phenomenon.

DOI: 10.1103/PhysRevB.107.214305

I. INTRODUCTION

Over the last decades, the high brightness achievable by x-ray synchrotron radiation light sources, together with their high-energy resolution and control of the polarization, gave an impressive boost to techniques capable of retrieving electronic and structural properties of matter. Nowadays, synchrotron spectroscopy is extensively used in a large number of scientific fields, ranging among condensed matter, organic and inorganic chemistry, nanotechnology, photocatalysis, and molecular biology. As an example, it is now routine to trace chemical reactions with x-ray absorption spectroscopy (XAS) and x-ray emission spectroscopy (XES) approaches, map the spin states via resonant effects in the dichroic response (e.g., Faraday or Kerr rotation), or detect molecular chirality [1–3].

More recently, time-resolved approaches combining synchrotrons and optical lasers have enabled the investigation of dynamic processes on a timescale of tens of picoseconds or longer [4–7], and generally with very low-energy synchrotron pulses. With the advent of ultrafast (<100 fs) sources like high-harmonic generation (HHG) laboratory lasers and free electron lasers (FELs), shorter timescales and higher pulse energies have become available. This has facilitated access to the dynamics of electronic band excitations [8–11], and high-resolution (tens of meV) time-resolved (Tr)-XAS/XES represents a strategic asset in the investigation of fundamental science, as well as for characterization of functional materials and catalytic applications [12,13].

HHG-based techniques suffer from low intensity at higher photon energy, such as the soft x-ray region. FELs provide much higher photon fluxes, but there are few sources, so that access is limited. The efficient use of FEL sources requires the implementation of novel approaches to spectroscopy, which benefit from the high-peak brightness and broad spectral bandwidth typical of FEL pulses. In this respect, it is highly desirable to develop multiplexing approaches capable of simultaneously exploiting a large spectral bandwidth without the need for spectral filtering and photon-energy scanning. An elegant and effective solution to multiplex-based spectroscopy is represented by correlation spectroscopy methods based on the determination of the statistical fluctuations introduced by the interaction of the light pulses with the sample; such

*deangelis@iom.cnr.it

approaches have been realized both in the optical region [14,15] as well as in the x-ray range [16–19].

Here we extend those techniques to the extreme ultraviolet (EUV) regime, and in particular to the $L_{2,3}$-edge (photon energy ≈100 eV), to investigate the structural and electronic dynamics of crystalline silicon (c-Si).

c-Si exhibits different photoinduced dynamics depending on the optical pump intensity and wavelength, especially if the excitation is above or below the direct conduction-band–valence-band energy gap. At low fluence ($<10\,\mathrm{mJ/cm^2}$) [20–22], i.e., when the laser-deposited energy does not modify the covalent nature of c-Si bonding and no phase transition is excited, the early response of the electronic structure to an external optical stimulus is characterized by the modification of the band-structure profile and density of states. State blocking based on the Pauli principle, broadening, and band-gap renormalization narrowing effects have been identified on the subpicosecond timescale [20]. At longer times, of the order of tens of picoseconds, i.e., when electron-phonon coupling transfers the electronic excitation energy to the crystal lattice, structural deformations, such as directional and isotropic thermal expansion, have been reported as additional relaxation processes [21,22]. At high fluence ($>170\ \mathrm{mJ/cm^2}$), when the deposited energy per atom is sufficient to modify the covalent nature of c-Si bonding, various experimental works indicated that the optical stimulus drives the c-Si band structure across a solid-liquid phase transition, occurring on the few-picosecond timescale [23–26]. Extensive investigation of nonthermal melting, from both theoretical [27–31] and experimental standpoints [32–34], have shown that after a few tens of picoseconds, the phase transition proceeds through a polymorphic evolution of the liquid phase, from an initial high-density disordered structure to another liquid phase with lower atomic coordination number [29,35]. At moderate fluence, i.e., before the onset of the solid-liquid phase transition, it has been predicted that a precursor state of the nonthermal melting process can be identified with the softening of interatomic bonds. This is described as a modification of the potential-energy landscape, that induces the instability of transverse and longitudinal acoustic phonons [27,36,37]. This bond softening (BSo) phenomenon has been experimentally observed for several classes of bulk materials after excitation with subpicosecond optical pulses, as a fluence-dependent temporal modulation of the intensity of Bragg spots in x-ray diffraction [38–41]. On freestanding polycrystalline Si membranes, an exponential decay of the x-ray-diffraction signal was first observed and interpreted as a heat-transfer dynamic on the atomic scale, characterized by a well-defined time constant [42]. These heating dynamics were later described by an *ab initio* simulation [36] in terms of a BSo. These authors calculated that the modification of the potential-energy landscape proceeds in a c-Si system through thermal phonon squeezing when excited below the Lindemann stability limit [43]. Moreover, they noted that the time constant associated with the phonon-squeezing process depends on the number of electron-hole pairs per unit volume that are generated by the laser pulse.

In this work, the combined XAS/XES analysis allowed us to observe the BSo on the timescale of electronic thermalization.

II. RESULTS

A. Experimental setup

The XAS/XES measurements were performed at the EIS-TIMEX beamline of the FERMI FEL facility in Trieste, Italy [44]. The beamline is optimized for pump-probe measurements; two spectrometers are available along the photon beam path (one upstream and the other downstream of the experimental chamber) and both of them can operate in single-shot mode at the FEL repetition rate (50 Hz). The first spectrometer, called PRESTO [45], is integrated in the FERMI photon transport system. It allows us to characterize the spectral content of each FEL pulse by imaging, in the energy-dispersive plane, the first diffraction order of a variable line-spacing grating. The second one, called WEST [46], is placed downstream of the TIMEX end station and is designed to collect the FEL photons transmitted by the sample. It comprises an EUV reflective grating and detector. The resolving power is 1×10^4 for PRESTO and 4×10^3 for WEST. The sample was an ultrapolished c-Si (001) *p*-doped membrane, 200-nm thick, purchased from Norcada.

We used the FERMI FEL-2 source [47] that was operated in the optical klystron mode (so-called "SASE-like" because of its similarity to the Self Amplified Stimulated Emission mode) [48]. This mode maximizes the radiation bandwidth, while achieving the stochastic ("spiky") spectral profile required by our analysis method (see Supplemental Material [49]). To fully cover the c-Si $L_{2,3}$ absorption edge, we scanned the photon energy of the SASE beam in five steps from 99.0 to 102.5 eV. Each step covered a distinct subregion of the absorption edge, with average central photon energies of 99.6, 99.8, 100.5, 101.0, and 101.6 eV. The SASE-like emission bandwidth was approximately 0.8 eV.

B. Static sample characterization

As a preliminary step, we performed XAS/XES measurements across the $L_{2,3}$ edge of c-Si. The results are shown in Fig. 1, where the colored boxes correspond to the different subregions of photon energy. As described in detail in the Supplemental Material, to retrieve information on the elastic (XAS) and the inelastic (XES) x-ray response of the sample, we collected 10^5 spectra for each of the aforementioned subregions of the photon-energy range. The sample response was evaluated using the Tikhonov regularization method [59] involving the transfer matrix connecting the ensemble of input and output spectra. These results were obtained with five acquisitions of about 20 min each at 50-Hz FEL repetition rate, and the time needed to change the FEL photon-energy range was about 2 min. The data analysis can be carried out online right after data acquisition.

In order to maximize the signal-to-noise ratio in the PRESTO and WEST spectrometers, we discard the FEL shots with very low intensity, i.e., when the recorded intensity on a spectrometer was barely visible above the noise level. In postprocessing filtering analysis, we calculated the average and the root-mean-square (rms) spectral intensity of the full dataset and applied a threshold filter to disregard all shots whose intensity was more than two times the variance lower than the average, i.e., approximately 2% of the total number of shots.

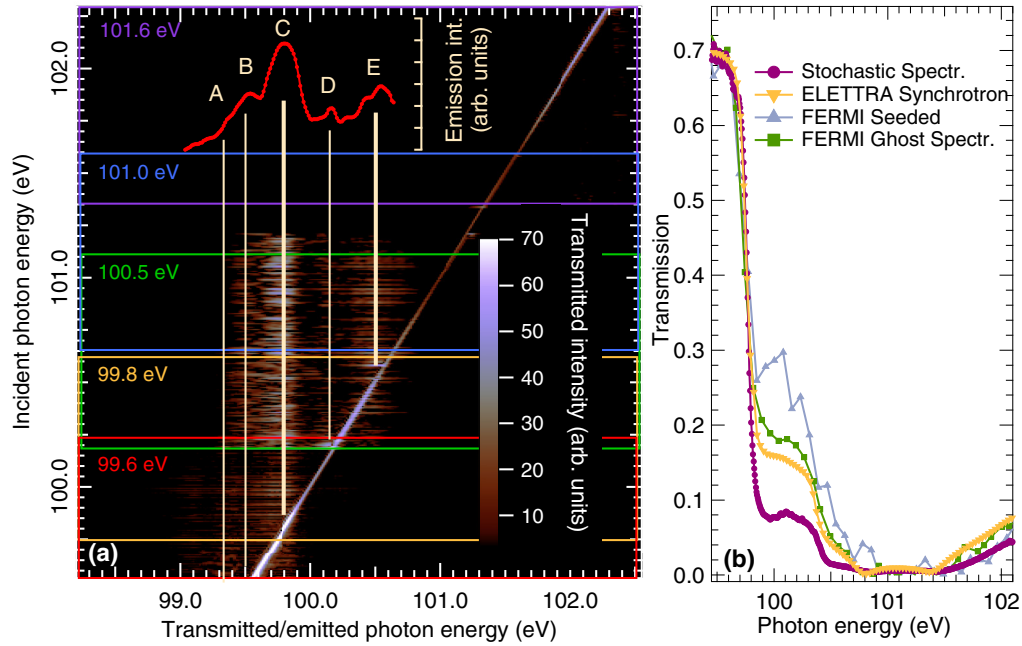

FIG. 1. (a) Reconstructed sample response map at equilibrium. Colored rectangles refer to the five photon-energy settings of the SASE-like emission (text labels with the same color indicate the average photon energy for each setting), while vertical white lines indicate the emission features. Inset in red represents the integrated emission spectrum; letters from A to E label the emission features. (b) Transmission profile of c-Si, as obtained from the diagonal terms of the sample response map (purple dots connected by lines; here, error bars are <2% and cannot be resolved on this scale), is compared to other spectroscopic methods, as detailed in the legend.

In Fig. 1(a), clear intensity modulations along the matrix diagonal are distinguishable. This corresponds to the sample response at the energy of the input radiation, i.e. the XAS spectrum across the c-Si edge.

Additional off-diagonal vertical features are observable in the upper triangular matrix. Those features correspond to x-ray emission processes as a result of electronic transitions from higher, occupied states into the core-holes created by input EUV photons. Emission lines are visible at about (A) 99.35, (B) 99.50, (C) 99.76, (D) 100.10, and (E) 100.45 eV. Lines C and E can be associated with the radiative deexcitation into the L_2 and L_3 orbitals. The complex x-ray emission spectrum is governed by multielectron interaction and core-hole screening effects, resulting from participation of the intermediate state in excitation and deexcitation processes. The faint series of emission lines at lower energies are in good agreement with the structures observed in Si nanoparticles by Šiller *et al.* [60]. They ascribe those features to Si in-gap states due to defects or doping, e.g., oxygen or carbon impurities, resulting in deeper donor states located ≈0.25 eV below the conduction-band minimum.

Figure 1(b) reports the integrated profile along the matrix diagonal (purple dots connected by lines). The spectrum clearly displays two EUV transmission drops assigned to the spin-orbit split resonances of the $2p$ levels at 99.76 eV (L_3 edge) and 100.45 eV (L_2 edge), corresponding, respectively, to emission features C and E. The present data are compared with (i) a spectrum from a nominally identical sample obtained by a synchrotron measurement (at the BEAR beamline of the Elettra synchrotron [61], yellow line) with comparable energy resolution and acquisition time; (ii) a measurement performed at FERMI by using narrow-band (seeded-mode) FEL emission and scanning the photon energy (gray line). It is worth noticing the lower-energy resolution of about 75 meV due to the reduced number of experimental points collected in the same acquisition time (2 h); and (iii) a measurement performed at FERMI (in SASE-like mode) obtained by exploiting the ghost spectroscopy method (green line) [18]: The energy and temporal resolution, as well as the acquisition time, are comparable.

Besides the remarkable data quality, we observed different ratios among the relative amplitude of the L_2 and L_3 edges in the four cases. This can be ascribed to the high sensitivity of this parameter to the chemical and structural environment of the Si atoms [62–65], added to the fact that the measurements were performed on different Si membranes, although nominally identical, that may have been affected by different contamination levels.

This comparison validates the correlation spectroscopy method of Kayser *et al.* [16] in the EUV regime, indicating that the energy resolution is superior to FEL data acquired by scanning the photon energy and comparable to standard synchrotron measurements operated with an x-ray monochromator. In addition, the present approach allows for the simultaneous characterization of occupied and unoccupied electronic states, thus providing more comprehensive information on the electronic configuration of the scattering system. Moreover, an important advantage with respect to synchrotron-based experiments is the use of an ultrafast EUV

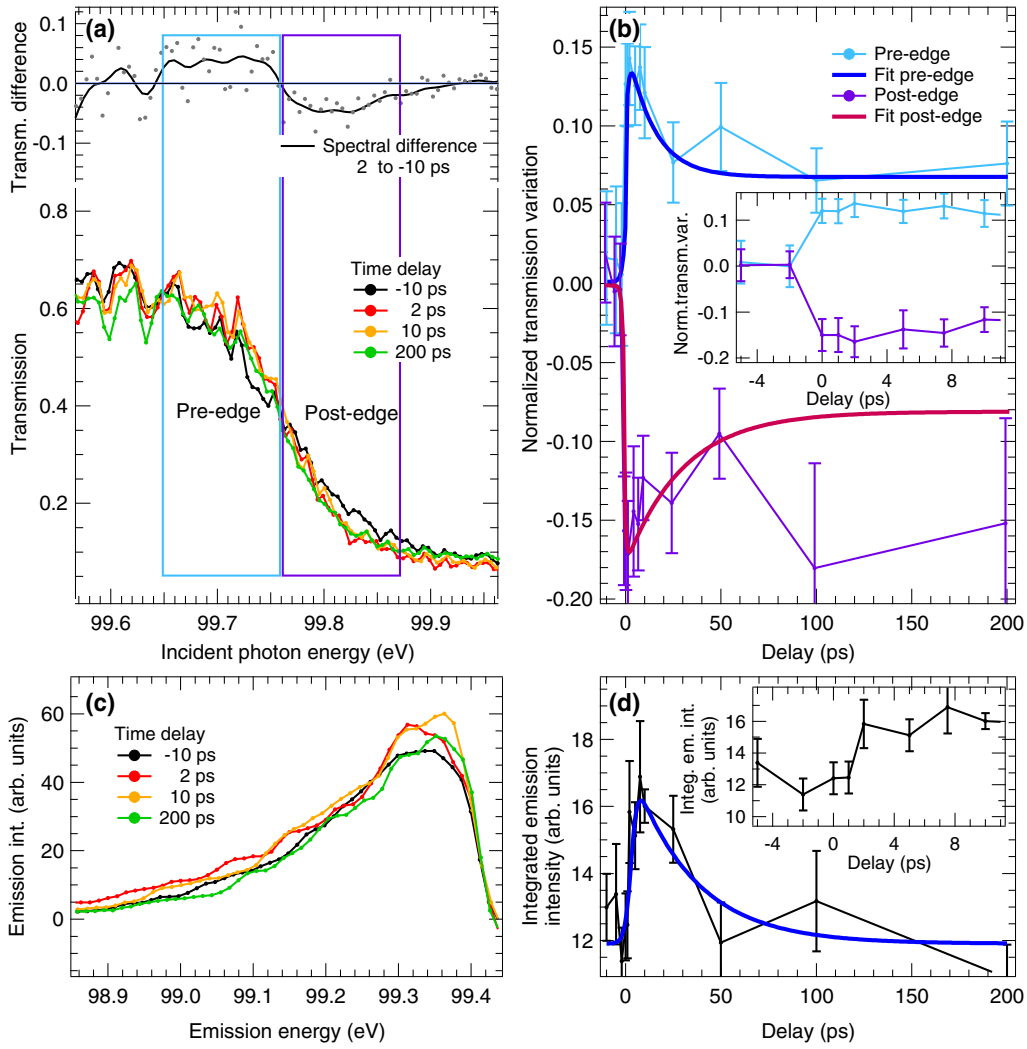

FIG. 2. (a) Selected transmission spectra before and after optical excitation, as indicated in the legend. Light blue and purple rectangles define the "preedge" (99.65–99.76 eV) and "postedge" (99.76–99.87 eV) spectral regions. (b) Light blue and purple data refer to the time dependence of the normalized variation of the transmitted intensity in the preedge and postedge regions, respectively; fit results are shown in the same plot. Inset shows an enlargement of the initial part of the dynamics. (c) Profiles of the emission line at 99.35 eV as a function of the delay, as indicated in the legend. (d) Time dependence of the total emission intensity at 99.35 eV: experimental data in black, fit result in blue. Inset shows an enlargement of the initial part of the dynamics.

source that can be used for time-resolved subpicosecond spectral investigations.

C. Laser-driven dynamics

We used EUV correlation spectroscopy in a time-resolved experiment to investigate the dynamics of c-Si after femtosecond optical excitation with 20- mJ/cm^2 fluence. This regime is below the damage threshold and has been theoretically described in the work of Zijlstra *et al.* [36] as a precursor to a nonthermal melting process. To photoexcite the c-Si sample, we employed an optical pulse with 3.16-eV photon energy (392-nm wavelength) and 90-fs pulse duration. A pump-probe time-delay scan consisted of about 20 time-delay points, from −5 to 250 ps, and at each point we acquired a dataset consisting of 50 000 SASE-like FEL shots. The FEL pulse duration was about 280 ± 30 fs full width at half maximum and it was the factor limiting the time resolution of our experiment. We focused on the Si L_3 edge, and we set the nominal SASE photon energy at 99.6 eV. The time needed to complete a scan was about 8 h, and at such moderate fluence levels, no sample damage during this time was observed during the experiment. To obtain Tr-XAS/XES profiles, the correlation analysis was performed for each time-delay dataset (more details in the Supplemental Material). Figure 2(a) shows the retrieved XAS profile at four selected time delays: Before (−10 ps) and after (+2, +25, and +200 ps) the optical excitation.

Two main features characterize the dynamics of the XAS spectra from the excited sample, namely an increase in the sample transmission before the absorption resonance and a decrease after it. Figure 2(b) reports the dynamics of the normalized XAS at the L_3 edge; the inset in Fig. 2(b) shows an enlargement of the first 10-ps dynamics. We can identify two distinct dynamics: (i) a rise (decrease) of the sample transmission in the pre- (post-)edge area in the first 2 ps after the excitation; and (ii) an inflection (increase) of the transmission

between 2 and 50 ps, slightly faster in the preedge region with respect to the postedge one, which progressively recovers the transmission of the sample before excitation.

To estimate the characteristic time constant for these dynamics, we fitted the two datasets with a model function defined as a logistic function attenuated by an exponential factor for positive delay values. From these fits, the exponential attenuation time is 15 ± 5 ps for the preedge and 20 ± 5 ps for the postedge. The rise (fall) time is beyond the intrinsic time resolution of our measurement, determined by the FEL pulse duration.

A dynamic effect was concurrently observed in the XES line at 99.35 eV (feature A), as displayed in Fig. 2(c). Here, selected emission spectra [integrated over the vertical energy dimension in Fig. 1(a)] are shown. The corresponding dynamics are reported in Fig. 2(d), where we observed an increase in the emission intensity in the first 10 ps after the excitation and a slower recovery on longer timescales. To analyze this dataset, we used the same fitting function described above: The rise time appears longer than the one observed in the transmission variation (2 ± 0.5 ps), while the recovery time constant is 22 ± 5 ps, which is similar to the time constant we observed in Tr-XAS.

III. DISCUSSION

The electronic and structural dynamics induced in Si by short laser pulses have been extensively investigated previously. Depending on the excitation fluence, different dynamical regimes have been recognized. At low fluence, below $10\,\mathrm{mJ/cm^2}$, thermal phenomena are more prominent than electronic ones, as discussed by Cushing *et al.* [22], where EUV spectroscopy is used to describe the hot phonon and carrier relaxation in c-Si excited by different femtosecond laser pulse in the range from infrared to ultraviolet. At 800-nm pumping wavelength, the authors observed a broadening of the absorption edge, which, to make a direct comparison with our results, can be described as a decrease (increase) of sample transmission in the preedge (after-edge) spectral region. They also modeled this effect using a density-functional theory approach. The observed dynamics were rationalized in terms of state filling, band-gap renormalization, and lattice deformation. However, in the present work we observe the opposite behavior of the L_3 edge (i.e., a narrowing of the edge after the excitation), indicating that the framework described by Cushing *et al.* is not compatible with our experiment, and that the larger pumping fluence in our case gives rise to nonthermal phenomena.

On the other hand, melting phenomena start to take place for pump fluence above $200\,\mathrm{mJ/cm^2}$. In this condition, Beye *et al.* [32] induced a nonthermal melting of Si in the first 2 ps, followed by a phase transition from a low-density liquid to a high-density liquid phase, observed 5 ps after the excitation. It is worth noting that the fluence used in that experiment is one order of magnitude higher than that used in the present experiment. At the fluence employed in the present experiment, we did not observe evidence of melting phenomena, neither from transmission measurements nor from microscopic inspection, despite the prolonged (several hours) exposure to the laser and FEL beams. This conclusion is endorsed by the experimental observation (by microscopic inspection and transmission measurement) of no visible sample damage even after 8 h of exposure to the pump pulse.

We exclude these two opposing pump-fluence regimes as valid interpretative frameworks and consider the calculations and the experimental observations reported by Zijlstra *et al.* [36]. On the basis of the excitation-fluence regime described there, we can infer that our pumping conditions were suited to induce BSo, i.e., the weakening of the potential-energy surface that indirectly generates an increase in the electronic density of states close to the conduction-band minimum. Those processes are schematically represented in Fig. 3 for preedge (a)–(c) and postedge (d)–(f) photon-energy condition, respectively, under the hypothesis that the band-gap energy (i.e., the energetic difference between the conduction-band (CB) minimum and the valence-band (VB) maximum) is unaffected by optical pumping.

Panels 3(a) and 3(d) describe the static situation and the main processes considered. At the preedge energy [Fig. 3(a)], i.e., for photon energy (E_{ph}) smaller than the energy of the core-level (CL) transition (E_{CL}), only electrons from the VB can be excited above the $\mathrm{CB_{min}}$, contributing to the XAS signal. On the other hand, since E_{ph} is smaller than E_{CL}, the absorption from the core level is suppressed. As a consequence, no XES signal can be expected, due to the lack of a core-hole required for such an electronic transition. The static situation is more complex for the postedge energy ($E_{\mathrm{ph}} > E_{\mathrm{CL}}$) [Fig. 3(d)]. Here, additionally to the processes described for the preedge case [not shown in Fig. 3(d)], the higher photon energy activates an absorption channel from the core level to the conduction band. The electrons excited by such an electronic transition, ultimately limited by the density of states in the CB, can quickly ($<$10 fs) deexcite to $\mathrm{CB_{min}}$ by means of inelastic intraband energy-loss processes. On the same timescale, the electronic vacancy in the core level (core-hole), generated by the absorption process, can be filled by the spontaneous emission of secondary photons (XES) involving either CB or VB electrons.

The Pauli blocking effects [65,66] induced by optical pumping (with photon energy larger than the band gap) are described in Figs. 3(b) and 3(e) for preedge and postedge situations, respectively. In these panels, no BSo is taken into account and no deformation of the VB and CB profiles is considered. Under such assumptions, for the preedge case [Fig 3(b)], the optical pump will excite electrons from the top of the VB to the bottom of the CB, and such a process is competitive with EUV absorption; indeed, the laser pump will fill empty states required for the EUV electronic transition. As a consequence, an increase of EUV sample transmission is expected [graphically represented by crossed dashed-dotted lines in Fig. 3(b) with respect to the stationary condition, Fig. 3(a)]. The same effects are expected for the postedge case depicted in Fig 3(e). In this case the laser pulse will populate states in the conduction band inducing a suppression of core-level absorption and, as a consequence of the reduced number of final states, a reduction of the XES signal. While the Pauli blocking effect phenomenologically reproduces the experimental observable in the XAS signal for the preedge condition, the opposite trend is observed for photon energy

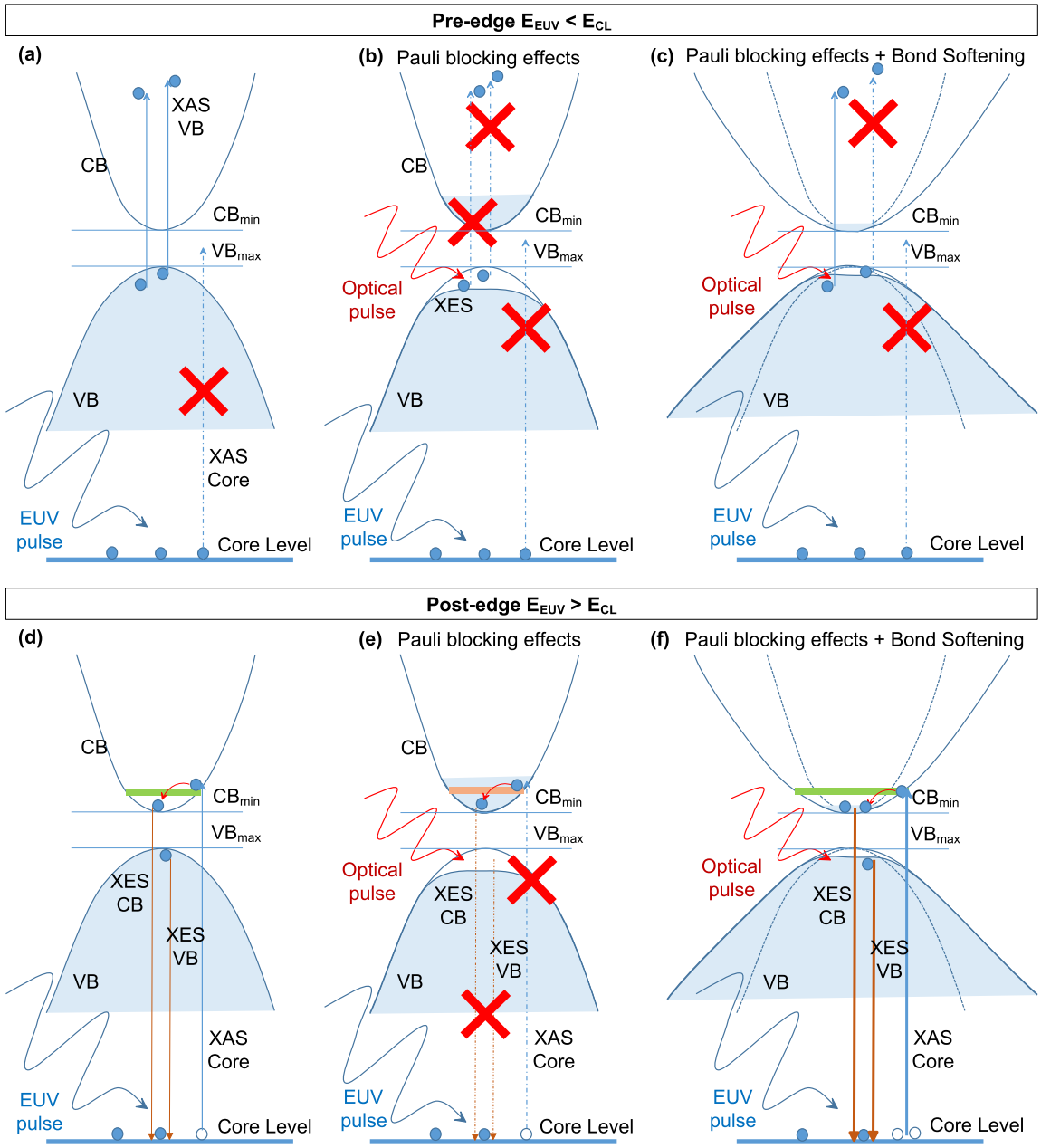

FIG. 3. Schematic representation of the electronic processes described in the text, related to EUV absorption. (a), (d) Static case, i.e., EUV absorption in the absence of the laser pump pulse, for EUV energies below and above the absorption edge (preedge and postedge), respectively. (b), (e) EUV absorption occurring after laser pump, in the absence of the BSo effect, for EUV energies below and above absorption edge, respectively). (c), (f) EUV absorption occurring after laser pump in the presence of the BSo effect, for EUV energies below and above absorption edge, respectively.

above the Si $L_{2,3}$ edge in the experimental XAS and XES time-resolved signals [Figs. 2(a) and 2(c)].

The effects of BSo in the electronic transition, after optical excitation, are represented in Figs. 3(c) and 3(f) for preedge and postedge EUV photon energy, respectively. In these figures, the BSo is represented as a weakening of the CB and VB energetic gradient (continuous blue lines for BSo case, dashed lines for static case). Such a variation of band profiles increases the density of the available states both above the CB_{min} and below the VB_{max}. As a consequence, for the preedge case [Fig 3(c)] the optically excited electrons from the VB will populate states in the CB closer to the CB_{min}, reducing the effects of Pauli blocking on EUV absorption. In the same way, the larger density of states induced by BSo will favor the CL transition for $E_{ph} > E_{CL}$ [Fig. 3(f)]. As a consequence, in the postedge case, BSo will produce an increase of sample absorption (measurable as a decrease of the sample transmission). Moreover, the larger number of generated core-holes will increase the probability of XES transitions from both the CB and VB, since a larger number of final states would be available. The above-described phenomenology of BSo with (1) a smaller decrease of sample XAS with respect to the Pauli

blocking process in the preedge region, and (2) an increase of both sample absorption and spontaneous emission rate in the postedge region fits well with the observed trend in the dynamics of unoccupied (XAS) and occupied (XES) states for c-Si $L_{2,3}$ edge reported in Figs. 2(a) and 2(c). Zijlstra *et al.* identify this BSo process as a precursor of the nonthermal melting of c-Si.

However, Zijlstra's investigation refers to the electronic dynamics occurring in the first picosecond after the pump. We instead explored the evolution of the system on the timescale of thermal phenomena driven by electron-phonon coupling: We observed a relatively fast recovery in the first 25 (50) ps, followed by slower dynamics. The excited and delocalized electrons created by the pump pulse are expected to occupy nonbonding and antibonding states in the conduction band and to weaken the atomic covalent bonds. In this time delay range we expect lattice modifications to take place during the system thermalization. Despite the different pumping fluence, we note that the ten-to-hundreds of picoseconds recovery dynamics we observe are similar to those reported by Beye *et al.* after the liquid-liquid phase transition.

Also, in the XES case, we observed an $\sim$50−ps recovery time, followed by a slower dynamic. From the latter observation we might infer that transmission and emission dynamics are related to the same electronic/structural phenomenon in the excited c-Si in the first 50 ps after the laser pulse. A detailed description of this specific phenomenon is beyond the scope of this work. Nevertheless, we think that our correlation spectroscopy approach provides great advantages in the investigation of electronic dynamics, due to its capability of extracting information from both occupied and unoccupied electronic states simultaneously.

IV. CONCLUSION

In this work we presented the implementation of correlation stochastic spectroscopy in the EUV regime, using SASE-like FEL pulses. We demonstrated the potential of this approach to overcome the efficiency issues of the FEL scan-based spectroscopy taking advantage of the spectral instability of SASE-like radiation. This allows us to reconstruct high-energy resolution XAS/XES spectra of c-Si. We used this approach to explore the dynamics of c-Si excited by optical radiation in a fluence regime below that needed to induce nonthermal melting. We interpreted the experimental findings in terms of the bond softening phenomenon, whose interest lies in the dynamic interplay between atomic bonding nature and electronic structure. We revealed that the loss of covalent bonding due to an optical excitation (392-nm-wavelength ultrashort pulses with 20- $\mathrm{mJ/cm^2}$ fluence) results in a distortion of the c-Si absorption edge, different from the one resulting from conventional heating of the Fermi-Dirac distribution [67–69], and also influences XES. This observation, while confirming the nonthermal nature of the photoinduced phase transformation in c-Si, indicates a rearrangement of the crystalline bonds occurring on the timescale of electron-phonon coupling.

Because of the inherent dynamic nature of this process, a time-resolved investigation technique is essential, and stochastic spectroscopy has proven to be effectively suited to this task.

In a more general context, EUV stochastic correlation spectroscopy provides comparable information with synchrotron-based measurements, in terms of acquisition time, signal-to-noise ratio, and energy resolution, with the valuable additional benefit of allowing time-resolved measurements with subpicosecond resolution and the simultaneous determination of XES response.

EUV correlation spectroscopy can be applied to dynamical studies of elastic and inelastic response in soft-matter samples, such as for example the selective enhancement of Raman modes in the aromatic ring of enantiomers [70,71]. By adding the control over the dichroic response, EUV correlation spectroscopy could also be exploited to study, e.g., the dynamics of spin magnons in antiferromagnetic structures [72], where high-energy resolution is necessary to extract valuable information on such inelastic processes.

Finally, it is worth mentioning that correlation-based spectroscopy techniques combined with subfemtosecond resolution might represent a valuable tool for attosecond science. Indeed, the majority of the Tr-XAS/XES setups use a monochromator, which inherently results in a pulse lengthening, and therefore can deteriorate the time resolution. On the other hand, it has been shown that approaches based on correlating the energy fluctuations within the emission bandwidth of a subfemtosecond pulse allows the statistical retrieval of the energy resolution, while potentially maintaining the subfemtosecond time resolution [73].

ACKNOWLEDGMENTS

We acknowledge FERMI staff for the support during the data collection campaign, in particular Luca Giannessi and Giuseppe Penco for the discussion on the optical klystron lasing scheme. J.S. acknowledges partial support from the National Science Centre (Poland) under Grant No. 2017/27/B/ST2/01890.

The authors declare no competing interests.

[1] P. M. Kraus, M. Zürch, S. K. Cushing, D. M. Neumark, and S. R. Leone, The ultrafast x-ray spectroscopic revolution in chemical dynamics, Nat. Rev. Chem. **2**, 82 (2018).

[2] U. Bergmann, J. Kern, R. W. Schoenlein, P. Wernet, V. K. Yachandra, and J. Yano, Using x-ray free-electron lasers for spectroscopy of molecular catalysts and metalloenzymes, Nat. Rev. Phys. **3**, 264 (2021).

[3] M. Hertzog, M. Wang, J. Mony, and K. Börjesson, Strong light–matter interactions: A new direction within chemistry, Chem. Soc. Rev. **48**, 937 (2019).

[4] S. Pascarelli, O. Mathon, T. Mairs, I. Kantor, G. Agostini, C. Strohm, S. Pasternak, F. Perrin, G. Berruyer, P. Chappelet, C. Clavela, and M. C. Dominguez, The time-resolved and extreme-conditions XAS (TEXAS) facility at the european synchrotron

radiation facility: The energy-dispersive X-ray absorption spectroscopy beamline ID24, J. Synchrotron Radiat. **23**, 353 (2016).

[5] N. Bergeard, M. G. Silly, D. Krizmancic, C. Chauvet, M. Guzzo, J. P. Ricaud, M. Izquierdo, L. Stebel, P. Pittana, R. Sergo, G. Cautero, G. Dufour, F. Rochete, and F. Sirotti, Time-resolved photoelectron spectroscopy using synchrotron radiation time structure, J. Synchrotron Radiat. **18**, 245 (2011).

[6] C. Bressler and M. Chergui, Ultrafast x-ray absorption spectroscopy, Chem. Rev. **104**, 1781 (2004).

[7] R. Geneaux, H. J. Marroux, A. Guggenmos, D. M. Neumark, and S. R. Leone, Transient absorption spectroscopy using high harmonic generation: A review of ultrafast x-ray dynamics in molecules and solids, Philos. Trans. R. Soc. A **377**, 20170463 (2019).

[8] W. Li, X. Zhou, R. Lock, S. Patchkovskii, A. Stolow, H. C. Kapteyn, and M. M. Murnane, Time-resolved dynamics in N_2O_4 probed using high harmonic generation, Science **322**, 1207 (2008).

[9] C. Behrens, F.-J. Decker, Y. Ding, V. A. Dolgashev, J. Frisch, Z. Huang, P. Krejcik, H. Loos, A. Lutman, T. J. Maxwell, J. Turner, J. Wang, M.-H. Wang, J. Welch, and J. Wu, Few-femtosecond time-resolved measurements of x-ray free-electron lasers, Nat. Commun. **5**, 3762 (2014).

[10] S. Hellmann, C. Sohrt, M. Beye, T. Rohwer, F. Sorgenfrei, M. Marczynski-Bühlow, M. Kalläne, H. Redlin, F. Hennies, M. Bauer, A. Föhlisch, L. Kipp, W. Wurth, and K. Rossnagel, Time-resolved x-ray photoelectron spectroscopy at FLASH, New J. Phys. **14**, 013062 (2012).

[11] C. Callegari, A. N. Grum-Grzhimailo, K. L. Ishikawa, K. C. Prince, G. Sansone, and K. Ueda, Atomic, molecular and optical physics applications of longitudinally coherent and narrow bandwidth free-electron lasers, Phys. Rep. **904**, 1 (2021).

[12] M. Maiuri, M. Garavelli, and G. Cerullo, Ultrafast spectroscopy: State of the art and open challenges, J. Am. Chem. Soc. **142**, 3 (2019).

[13] J. Lloyd-Hughes, P. M. Oppeneer, T. P. Dos Santos, A. Schleife, S. Meng, M. A. Sentef, M. Ruggenthaler, A. Rubio, I. Radu, M. Murnane, X. Shi, H. Kapteyn, B. Stadtmüller, K. M. Dani, F. H. da Jornada, E. Prinz, M. Aeschlimann, R. L. Milot, M. Burdanova, J. Boland *et al.*, The 2021 ultrafast spectroscopic probes of condensed matter roadmap, J. Phys.: Condens. Matter **33**, 353001 (2021).

[14] J. O. Tollerud, G. Sparapassi, A. Montanaro, S. Asban, F. Glerean, F. Giusti, A. Marciniak, G. Kourousias, F. Billè, F. Cilento, S. Mukamel, and D. Fausti, Femtosecond covariance spectroscopy, Proc. Natl. Acad. Sci. USA **116**, 5383 (2019).

[15] G. Sparapassi, S. M. Cavaletto, J. Tollerud, A. Montanaro, F. Glerean, A. Marciniak, F. Giusti, S. Mukamel, and D. Fausti, Transient measurement of phononic states with covariance-based stochastic spectroscopy, Light Sci Appl. **11**, 44 (2022).

[16] Y. Kayser, C. Milne, P. Juranić, L. Sala, J. Czapla-Masztafiak, R. Follath, M. Kavčič, G. Knopp, J. Rehanek, W. Błachucki, M. G. Delcey, M. Lundberg, K. Tyrała, D. Zhu, R. Alonso-Mori, R. Abela, J. Sá, and J. Szlachetko, Core-level nonlinear spectroscopy triggered by stochastic x-ray pulses, Nat. Commun. **10**, 4761 (2019).

[17] Y. Klein, O. Sefi, H. Schwartz, and S. Shwartz, Chemical element mapping by x-ray computational ghost fluorescence, Optica **9**, 63 (2022).

[18] Y. Klein, A. K. Tripathi, E. Strizhevsky, F. Capotondi, D. De Angelis, L. Giannessi, M. Pancaldi, E. Pedersoli, K. C. Prince, O. Sefi, Y. Y. Kim, I. A. Vartanyants, and S. Shwartz, High-spectral resolution absorption measurements with free-electron lasers using ghost spectroscopy, Phys. Rev. A **107**, 053503 (2023).

[19] F. D. Fuller, A. Loukianov, T. Takanashi, D. You, Y. Li, K. Ueda, T. Fransson, M. Yabashi, T. Katayama, T.-C. Weng, R. Alonso-Mori, U. Bergmann, J. Kern, V. K. Yachandra, P. Wernet, and J. Yano, Resonant x-ray emission spectroscopy from broadband stochastic pulses at an x-ray free electron laser, Commun. Chem. **4**, 84 (2021).

[20] M. Schultze, K. Ramasesha, C. D. Pemmaraju, S. A. Sato, D. Whitmore, A. Gandman, J. S. Prell, L. J. Borja, D. Prendergast, K. Yabana, D. M. Neumark, and S. R. Leone, Attosecond band-gap dynamics in silicon, Science **346**, 1348 (2014).

[21] S. K. Cushing, M. Zürch, P. M. Kraus, L. M. Carneiro, A. Lee, H.-T. Chang, C. J. Kaplan, and S. R. Leone, Hot phonon and carrier relaxation in Si (100) determined by transient extreme ultraviolet spectroscopy, Struct. Dyn. **5**, 054302 (2018).

[22] S. K. Cushing, A. Lee, I. J. Porter, L. M. Carneiro, H.-T.Chang, M. Zürch, and S. R. Leone, Differentiating photoexcited carrier and phonon dynamics in the Δ, L, and Γ valleys of Si (100) with transient extreme ultraviolet spectroscopy, J. Phys. Chem. C **123**, 3343 (2019).

[23] C. V. Shank, R. Yen, and C. Hirlimann, Time-resolved Reflectivity Measurements of Femtosecond-Optical-Pulse-Induced Phase Transitions in Silicon, Phys. Rev. Lett. **50**, 454 (1983).

[24] H. W. K. Tom, G. D. Aumiller, and C. H. Brito-Cruz, Time-Resolved Study of Laser-Induced Disorder of Si Surfaces, Phys. Rev. Lett. **60**, 1438 (1988).

[25] K. Sokolowski-Tinten and D. von der Linde, Generation of dense electron-hole plasmas in silicon, Phys. Rev. B **61**, 2643 (2000).

[26] S. L. Johnson, P. A. Heimann, A. M. Lindenberg, H. O. Jeschke, M. E. Garcia, Z. Chang, R. W. Lee, J. J. Rehr, and R. W. Falcone, Properties of Liquid Silicon Observed by Time-Resolved X-Ray Absorption Spectroscopy, Phys. Rev. Lett. **91**, 157403 (2003).

[27] P. Stampfli and K. H. Bennemann, Time dependence of the laser-induced femtosecond lattice instability of Si and GaAs: Role of longitudinal optical distortions, Phys. Rev. B **49**, 7299 (1994).

[28] P. L. Silvestrelli, A. Alavi, M. Parrinello, and D. Frenkel, *Ab Initio* Molecular Dynamics Simulation of Laser Melting of Silicon, Phys. Rev. Lett. **77**, 3149 (1996).

[29] N. Medvedev, Z. Li, and B. Ziaja, Thermal and nonthermal melting of silicon under femtosecond x-ray irradiation, Phys. Rev. B **91**, 054113 (2015).

[30] K. Zhang, H. Li, and Y. Y. Jiang, Liquid–liquid phase transition in quasi-two-dimensional supercooled silicon, Phys. Chem. Chem. Phys. **16**, 18023 (2014).

[31] S. Sastry and C. Austen Angell, Liquid–liquid phase transition in supercooled silicon, Nat. Mater. **2**, 739 (2003).

[32] M. Beye, F. Sorgenfrei, W. F. Schlotter, W. Wurth, and A. Föhlisch, The liquid-liquid phase transition in silicon revealed by snapshots of valence electrons, Proc. Natl. Acad. Sci. USA **107**, 16772 (2010).

[33] N. J. Hartley, J. Grenzer, L. Huang, Y. Inubushi, N. Kamimura, K. Katagiri, R. Kodama, A. Kon, W. Lu, M. Makita,

T. Matsuoka, S. Nakajima, N. Ozaki, T. Pikuz, A. V. Rode, D. Sagae, A. K. Schuster, K. Tono, K. Voigt, J. Vorberger *et al.*, Using Diffuse Scattering to Observe X-Ray-Driven Nonthermal Melting, Phys. Rev. Lett. **126**, 015703 (2021).

[34] P. McMillan, M. Wilson, D. Daisenberger, and D. Machon, A density-driven phase transition between semiconducting and metallic polyamorphs of silicon, Nat. Mater. **4**, 680 (2005).

[35] S. Zhang, L. M. Wang, X. Zhang, L. Qi, S. Zhang, M. Ma, and R. Liu, Polymorphism in glassy silicon: Inherited from liquid-liquid phase transition in supercooled liquid, Sci. Rep. **5**, 8590 (2015).

[36] E. S. Zijlstra, A. Kalitsov, T. Zier, and M. E. Garcia, Squeezed Thermal Phonons Precurse Nonthermal Melting of Silicon as a Function of Fluence, Phys. Rev. X **3**, 011005 (2013).

[37] S. Hunsche, K. Wienecke, T. Dekorsy, and H. Kurz, Impulsive Softening of Coherent Phonons in Tellurium, Phys. Rev. Lett. **75**, 1815 (1995).

[38] E. S. Zijlstra, J. Walkenhorst, and M. E. Garcia, Anharmonic Noninertial Lattice Dynamics during Ultrafast Nonthermal Melting of InSb, Phys. Rev. Lett. **101**, 135701 (2008).

[39] V. Recoules, J. Clérouin, G. Zérah, P. M. Anglade, and S. Mazevet, Effect of Intense Laser Irradiation on the Lattice Stability of Semiconductors and Metals, Phys. Rev. Lett. **96**, 055503 (2006).

[40] S. L. Johnson, P. Beaud, E. Vorobeva, C. J. Milne, É. D. Murray, S. Fahy, and G. Ingold, Directly Observing Squeezed Phonon States with Femtosecond X-Ray Diffraction, Phys. Rev. Lett. **102**, 175503 (2009).

[41] N. S. Grigoryan, E. S. Zijlstra, and M. E. Garcia, Electronic origin of bond softening and hardening in femtosecond-laser-excited magnesium, New J. Phys. **16**, 013002 (2014).

[42] M. Harb, R. Ernstorfer, T. Dartigalongue, C. T. Hebeisen, R. E. Jordan, and R. D. Miller, Carrier relaxation and lattice heating dynamics in silicon revealed by femtosecond electron diffraction, J. Phys. Chem. B **110**, 25308 (2006).

[43] C. Chakravarty, P. G. Debenedetti, and F. H. Stillinger, Lindemann measures for the solid-liquid phase transition, J. Chem. Phys. **126**, 204508 (2007).

[44] C. Masciovecchio, A. Battistoni, E. Giangrisostomi, F. Bencivenga, E. Principi, R. Mincigrucci, R. Cucini, A. Gessini, F. D'Amico, R. Borghes *et al.*, EIS: The scattering beamline at FERMI, J. Synchrotron Radiat. **22**, 553 (2015).

[45] C. Svetina, D. Cocco, N. Mahne, L. Raimondi, E. Ferrari, and M. Zangrando, PRESTO, the on-line photon energy spectrometer at FERMI: Design, features and commissioning results, J. Synchrotron Radiat. **23**, 35 (2016).

[46] E. Principi, C. Svetina, D. De Angelis *et al.*, A versatile wide energy range spectrometer for soft X-ray FELs, Nucl. Instrum. Methods Phys. Res. Sec. A (NIM-A) (unpublished).

[47] E. Roussel, E. Allaria, C. Callegari, M. Coreno, R. Cucini, S. Di Mitri, B. Diviacco, E. Ferrari, P. Finetti, D. Gauthier, G. Penco, L. Raimondi, C. Svetina, M. Zangrando, A. Beckmann, L. Glaser, G. Hartmann, F. Scholz, J. Seltmann, I. Shevchuk *et al.*, Polarization characterization of soft x-ray radiation at FERMI FEL-2, Photon. **4**, 29 (2017).

[48] G. Penco, E. Allaria, G. De Ninno, E. Ferrari, and L. Giannessi, Experimental Demonstration of Enhanced Self-Amplified Spontaneous Emission by an Optical Klystron, Phys. Rev. Lett. **114**, 013901 (2015).

[49] See Supplemental Material at http://link.aps.org/supplemental/10.1103/PhysRevB.107.214305 for the details about data acquisition and analysis procedures; Tikhonov regularization method; and preliminary characterization of the FEL source in stochastic emission mode. It also contains Refs. [50–58].

[50] T. J. Lane and D. Ratner, What are the advantages of ghost imaging? Multiplexing for x-ray and electron imaging, Opt. Express **28**, 5898 (2020).

[51] O. Y. Gorobtsov, G. Mercurio, F. Capotondi, P. Skopintsev, S. Lazarev, I. A. Zaluzhnyy, M. B. Danailov, M. Dell'Angela, M. Manfredda, E. Pedersoli, L. Giannessi, M. Kiskinova, K. C. Prince, W. Wurth, and I. A. Vartanyants, Seeded x-ray free-electron laser generating radiation with laser statistical properties, Nat. Commun. **9**, 4498 (2018).

[52] R. J. Glauber, The quantum theory of optical coherence, Phys. Rev. **130**, 2529 (1963).

[53] A. Singer, U. Lorenz, F. Sorgenfrei, N. Gerasimova, J. Gulden, O. M. Yefanov, R. P. Kurta, A. Shabalin, R. Dronyak, R. Treusch, V. Kocharyan, E. Weckert, W. Wurth, and I. A. Vartanyants, Hanbury Brown and Twiss Interferometry at a Free-Electron Laser, Phys. Rev. Lett. **111**, 034802 (2013); **117**, 239903(E) (2016).

[54] C. Gutt, P. Wochner, B. Fischer, H. Conrad, M. Castro-Colin, S. Lee, F. Lehmkuhler, I. Steinke, M. Sprung, W. Roseker, D. Zhu, H. Lemke, S. Bogle, P. H. Fuoss, G. B. Stephenson, M. Cammarata, D. M. Fritz, A. Robert, and G. Grübel, Single Shot Spatial and Temporal Coherence Properties of the SLAC Linac Coherent Light Source in the Hard X-Ray Regime, Phys. Rev. Lett. **108**, 024801 (2012).

[55] O. Y. Gorobtsov, G. Mercurio, G. Brenner, U. Lorenz, N. Gerasimova, R. P. Kurta, F. Hieke, P. Skopintsev, I. Zaluzhnyy, S. Lazarev, D. Dzhigaev, M. Rose, A. Singer, W. Wurth, and I. A. Vartanyants, Statistical properties of a free-electron laser revealed by Hanbury Brown-Twiss interferometry, Phys. Rev. A **95**, 023843 (2017).

[56] I. A. Vartanyants and R. Khubbutdinov, Theoretical analysis of Hanbury Brown and Twiss interferometry at soft-x-ray free-electron lasers, Phys. Rev. A **104**, 023508 (2021).

[57] P. Pääkkönen, J. Turunen, P. Vahimaa, A. T. Friberg, and F. Wyrowski, Partially coherent Gaussian pulses, Opt. Commun. **204**, 53 (2002).

[58] H. Lajunen, J. Tervo, and P. Vahimaa, Theory of spatially and spectrally partially coherent pulses, J. Opt. Soc. Am. A **22**, 1536 (2005).

[59] D. Calvetti, S. Morigi, L. Reichel, and F. Sgallari, Tikhonov regularization and the L-curve for large discrete ill-posed problems, J. Comput. Appl. Math. **123**, 423 (2000).

[60] L. Šiller, S. Krishnamurthy, L. Kjeldgaard, B. R. Horrocks, Y. Chao, A. Houlton, A. K. Chakraborty, and M. R. C. Hunt, Core and valence exciton formation in x-ray absorption, x-ray emission and x-ray excited optical luminescence from passivated Si nanocrystals at the Si $L_{2,3}$ edge, J. Phys.: Condens. Matter **21**, 095005 (2009).

[61] L. Pasquali, A. De Luisa, and S. Nannarone, The UHV experimental chamber for optical measurements (reflectivity and absorption) and angle resolved photoemission of the BEAR Beamline at ELETTRA, AIP Conf. Proc. **705**, 1142 (2004).

[62] P. E. Batson, Silicon $L_{2,3}$ near-edge fine structure in confined volumes, Ultramicroscopy **50**, 1 (1993).

[63] T. van Buuren, L. N. Dinh, L. L. Chase, W. J. Siekhaus, I. Jimenez, L. J. Terminello, M. Grush, T. A. Callcoti, and J. A. Carlisle, Soft x-ray emission studies of the electronic structure in silicon nanoclusters, Mater. Res. Soc. Symp. Proc. **452**, 171 (1997).

[64] M. Schade, B. Fuhrmann, A. Chassé, F. Heyroth, M. Roczen, and H. S. Leipner, Distinction between morphous and crystalline silicon by means of electron energy-loss spectroscopy, Appl. Phys. A **120**, 393 (2015).

[65] F. Cummings, B. van Heerden, C. Arendse, and T. Muller, Electron energy loss spectroscopy and energy filtered transmission electron microscopy of hydrogenated nano-crystalline Si thin films deposited via hydrogen profiling during hot-wire CVD for application in photovoltaics, Mater. Today: Proc. **36**, 256 (2021).

[66] C. Trovatello, F. Katsch, M. Selig Borys, K. Yao, R. Borrego-Varillas, F. Scotognella, I. Kriegel, A. Yan, A. Zettl, P. J. Schuck, A. Knorr, Cerullo G, and S. Dal Conte, The ultrafast onset of exciton formation in 2D semiconductors, Nat. Commun. **11**, 5277 (2020).

[67] B. Rösner, B. Vodungbo, V. Chardonnet, F. Döring, V. A. Guzenko, M. Hennes, A. Kleibert, M. Lebugle, J. Lüning, N. Mahne, A. Merhe, D. Naumenko, I. P. Nikolov, I. Lopez-Quintas, E. Pedersoli, P. R. Ribič, T. Savchenko, B. Watts, M. Zangrando, F. Capotondi *et al.*, Simultaneous two-color snapshot view on ultrafast charge and spin dynamics in a Fe-Cu-Ni tri-layer, Struct. Dyn. **7**, 054302 (2020).

[68] E. Principi, E. Giangrisostomi, R. Mincigrucci, M. Beye, G. Kurdi, R. Cucini, A. Gessini, F. Bencivenga, and C. Masciovecchio, Extreme ultraviolet probing of nonequilibrium dynamics in high energy density germanium, Phys. Rev. B **97**, 174107 (2018).

[69] E. Principi, S. Krylow, M. E. Garcia, A. Simoncig, L. Foglia, R. Mincigrucci, G. Kurdi, A. Gessini, F. Bencivenga, A. Giglia, S. Nannarone, and C. Masciovecchio, Atomic and Electronic Structure of Solid-Density Liquid Carbon, Phys. Rev. Lett. **125**, 155703 (2020).

[70] S. Gómez, N. Rojas-Valencia, T. Giovannini, A. Restrepo, and C. Cappelli, Ring vibrations to sense anionic ibuprofen in aqueous solution as revealed by resonance Raman, Molecules **27**, 442 (2022).

[71] R. Mincigrucci, J. Rouxel, B. Rossi, E. Principi, C. Bottari, S. Catalini, D. Fainozzi, L. Foglia, A. Simoncig, A. Matruglio, G. Kurdi, F. Capotondi, E. Pedersoli, A. Perucchi, F. Piccirilli, A. Gessini, M. Giarola, G. Mariotto, S. Mukamel, F. Bencivenga *et al.*, Element- and enantiomer-selective visualization of molecular motion in real-time, Nat. Commun. **14**, 386 (2023).

[72] E. Rongione, O. Gueckstock, M. Mattern, O. Gomonay, H. Meer, C. Schmitt, R. Ramos, T. Kikkawa, M. Mičica, E. Saitoh, J. Sinova, H. Jaffrès, J. Mangeney, S. T. B. Goennenwein, S. Geprägs, T. Kampfrath, M. Kläui, M. Bargheer, T. S. Seifert, S. Dhillon, and R. Lebrun, Emission of coherent THz magnons in an antiferromagnetic insulator triggered by ultrafast spin-phonon interactions, Nat. Commun. **14**, 1818 (2023).

[73] T. Driver, S. Li, E. G. Champenois, J. Duris, D. Ratner, T. J. Lane, P. Rosenberger, A. Al-Haddad, V. Averbukh, T. Barnard, N. Berrah, C. Bostedt, P. H. Bucksbaum, R. Coffee, L. F. Di Mauro, L. Fang, D. Garratt, A. Gatton, Z. Guo, G. Hartmann *et al.*, Attosecond transient absorption spooktroscopy: A ghost imaging approach to ultrafast absorption spectroscopy, Phys. Chem. Chem. Phys. **22**, 2704 (2020).